

# Sum rule analysis of vector and axial-vector spectral functions with excited states in vacuum

Paul M. Hohler\* and Ralf Rapp†

*Cyclotron Institute and Department of Physics and Astronomy,  
Texas A&M University, College Station, TX 77843-3366, USA*

We simultaneously analyze vector and axial-vector spectral functions in vacuum using hadronic models constrained by experimental data and the requirement that Weinberg-type sum rules are satisfied. Upon explicit inclusion of an excited vector state, *viz.*  $\rho'$ , and the requirement that the perturbative continua are degenerate in vector and axial-vector channels, we deduce the existence of an excited axial-vector resonance state,  $a'_1$ , in order that the Weinberg sum rules are satisfied. The resulting spectral functions are further tested with QCD sum rules.

## I. INTRODUCTION

Chiral symmetry is believed to be a fundamental symmetry of QCD. However, this symmetry is spontaneously broken at low temperatures and chemical potentials by a finite expectation value of the quark (or chiral) condensate,  $\langle 0|\bar{q}q|0\rangle \simeq -2\text{fm}^{-3}$  per light quark flavor in vacuum. At higher temperatures, the symmetry is expected to be restored as the value of the condensate approaches zero. Such behavior has been observed in lattice-QCD computations [1, 2], but it remains a long-standing goal to observe chiral restoration in experiment. This is difficult because a direct measurement of the chiral condensate is not possible.

One way to indirectly infer the chiral condensate and deduce chiral symmetry restoration is through the use of sum rules. They are formulated to relate hadronic spectral functions to properties of the ground state (condensates) including chiral order parameters. The observation of in-medium changes of hadronic spectral functions can then signal pertinent changes in these order parameters. Of particular interest are spectral functions of so-called chiral partners, *i.e.*, hadronic states which are degenerate at chiral restoration, but are split in vacuum due to dynamical chiral breaking. The prime example are the iso-vector vector and axial-vector channels which are connected through Weinberg-type sum rules [3–5] (see, *e.g.*, Ref. [6] for a recent study of chiral partners in the open-charm sector). Therefore an accurate measurement of both the vector and axial-vector spectral functions can be used to infer chiral order parameters and thus “observe” chiral symmetry restoration. Additional information can be gleaned from the spectral functions by considering QCD sum rules [7, 8] which are dependent on both chirally symmetric and chirally breaking ground-state properties. A lot has been learned about the in-medium vector spectral function from dilepton measurements and their interpretation [9, 10], but no experimental measurement of the in-medium axial-vector spectral function has been performed to date. One is thus left with constructing effective models of the axial-vector spectral function in order to study chiral symmetry restoration.

In order to reliably evaluate in-medium effects on the vector and axial-vector spectral functions, one should first control their properties in vacuum. This is aided by accurate experimental measurements of the vacuum spectral functions through  $\tau$ -decays by the ALEPH and OPAL Collaborations [11, 12]. On the one hand, sum rules have been used along with experimental data to calculate the condensates [13–15]. On the other hand, the condensates can be used to constrain the spectral functions. Weinberg’s original study assumed a  $\delta$ -function approximation for both the low-lying vector and axial-vector resonances in his sum rules to determine the famous relation between the masses of the  $\rho$  and  $a_1$  mesons,  $m_{a_1} = \sqrt{2}m_\rho$  [3]. Similarly, QCD sum rules have been applied in the vector channel, where early works approximated the  $\rho$  by a  $\delta$  function while also considering medium effects [16, 17]. More recent work has considered spectral functions with a Breit-Wigner shape for the  $\rho$  peak [18], and have included the axial-vector channel in their analyses [19–21], while others analyzed calculations based upon a microscopic theory [20–23]. Clearly, the focus in previous work was on QCD sum rules, with the contribution to the continuum approximated by a  $\theta$ -function with a threshold energy. Furthermore, until the most recent studies [20, 21], the vacuum spectral functions did not take advantage of the high-precision  $\tau$ -decay data. The often simplified constructions of spectral functions used to analyze the sum rules, and the dearth of analyses to include the axial-vector channel or consider the Weinberg-type sum rules, leaves this area open for further considerations.

---

\*Electronic address: pmhohler@comp.tamu.edu

†Electronic address: rapp@comp.tamu.edu

In the present paper, we simultaneously analyze vector and axial-vector spectral functions in vacuum using an extended model which combines a microscopic  $\rho$  spectral function with Breit-Wigner ansätze for the  $a_1$  and the first excited states. This model is quantitatively constrained by both the experimental  $\tau$ -decays [11, 12] and the Weinberg-type sum rules [3–5]. By using this combination of criteria, the model may be considered a non-trivial fit of the data. Novel features of our analysis include the study of excited states and the postulate that the continuum contribution is identical for both the vector and axial-vector channels, as should be the case in the perturbative regime. In particular, the use of the Weinberg-type sum rules leads us to deduce the presence of an excited axial-vector state, about which rather little is known to date [24]. As an additional check, we utilize the constructed spectral functions in a pertinent analysis of QCD sum rules.

The outline of this paper is as follows. In Sec. II, the sum rules used in our investigation are introduced. In Sec. III, we detail the main ingredients to the vector and axial-vector spectral functions. Section IV presents the results of our fitting procedure and discusses our main findings in the context of Weinberg sum rules. In Sec. V, the constructed spectral functions are implemented into QCD sum rules, and we conclude in Sec. VI.

## II. WEINBERG AND QCD SUM RULES

Sum rules are a valuable tool for understanding non-perturbative aspects of QCD as they relate two different formulations of the same correlation function to each other. For the current paper, we will focus on two classes of sum rules, Weinberg-type and QCD sum rules.

Let us begin by defining the current-current correlators for the vector and axial-vector channels,

$$\Pi_V^{\mu\nu}(q) = -i \int d^4x e^{iqx} \langle T j_V^\mu(x) j_V^\nu(0) \rangle, \quad (1)$$

$$\Pi_A^{\mu\nu}(q) = -i \int d^4x e^{iqx} \langle T j_A^\mu(x) j_A^\nu(0) \rangle, \quad (2)$$

where  $j_V^\mu = \frac{1}{2} (\bar{u}\gamma^\mu u - \bar{d}\gamma^\mu d)$  and  $j_A^\mu = \frac{1}{2} (\bar{u}\gamma^\mu\gamma_5 u - \bar{d}\gamma^\mu\gamma_5 d)$  are the pertinent currents in the quark basis. The correlators can be decomposed into 4-dimensional transverse and longitudinal parts as

$$\Pi_{V,A}^{\mu\nu}(q^2) = \left( -g^{\mu\nu} + \frac{q^\mu q^\nu}{q^2} \right) \Pi_{V,A}^T(q^2) + \frac{q^\mu q^\nu}{q^2} \Pi_{V,A}^L(q^2). \quad (3)$$

Since the vector current is conserved,  $\Pi_V^L = 0$ . The longitudinal component of the axial-vector is governed by the contribution from the pion which causes the axial current not to be conserved. In vacuum, the self-energy of the pion is assumed to be negligible, rendering the imaginary part of the longitudinal axial-vector polarization of the simple form

$$\text{Im}\Pi_A^L(s) = -\pi f_\pi^2 s \delta(s - m_\pi^2) \quad (4)$$

with  $s = q^2$ .

It is also useful to define an additional polarization function,  $\bar{\Pi}_A(q^2) \equiv \Pi_A^T(q^2) + \Pi_A^L(q^2)$  (which corresponds to  $\Pi_A^2$  in Ref. [8]). The transverse polarization functions for both vector and axial-vector channels are used to define the spectral functions such that

$$\rho_V(q^2) \equiv -\frac{1}{\pi} \text{Im}\Pi_V^T(q^2), \quad (5)$$

$$\rho_A(q^2) \equiv -\frac{1}{\pi} \text{Im}\Pi_A^T(q^2). \quad (6)$$

A spectral function for  $\bar{\Pi}_A$  can be defined in a similar manner as

$$\bar{\rho}_A(q^2) \equiv -\frac{1}{\pi} \text{Im}\bar{\Pi}_A(q^2). \quad (7)$$

From the definition of  $\bar{\Pi}_A$  and Eqs. (4) and (6), we see that  $\bar{\rho}_A(s) = \rho_A(s) + f_\pi^2 s \delta(s - m_\pi^2)$ , *i.e.*, this spectral function has contributions from both the pion and the axial-vector mesons (plus continuum, see below).

The Weinberg-type sum rules characterize moments of the difference between the vector and axial-vector spectral functions, thereby quantifying the effects of chiral symmetry breaking. They have the general form

$$\int_0^\infty ds s^n \Delta\rho(s) = f_n, \quad (8)$$

where  $\Delta\rho \equiv \rho_V - \rho_A$ ,  $n$  is an integer, and  $f_n$  are chiral order parameters dependent on the sum rule in question.

The first two of these sum rules were originally derived by Weinberg [3] (hence the name for the class of sum rules) using current algebra arguments. They read

$$\text{(WSR 1)} \quad \int_0^\infty ds \frac{\Delta\rho(s)}{s} = f_\pi^2, \quad (9)$$

$$\text{(WSR 2)} \quad \int_0^\infty ds \Delta\rho(s) = f_\pi^2 m_\pi^2 = -2m_q \langle \bar{q}q \rangle, \quad (10)$$

and correspond to  $n = -1$  and  $n = 0$  in Eq. (8). Here,  $m_q \simeq 5$  MeV refers to the average current light-quark mass, while the Gellmann-Oaks-Renner relation [25],

$$f_\pi^2 m_\pi^2 = -2m_q \langle \bar{q}q \rangle, \quad (11)$$

was used to obtain the second equality in Eq. (10). In Weinberg's original work, the chiral limit was considered; here we have included terms linear in the quark mass [26–29]. Corrections to higher powers in  $m_q$  [26–28, 30] are expected to be small.<sup>1</sup> One sees that the chiral condensate can be calculated using Eq. (10) should both the vector and axial-vector spectral functions be known precisely. The sum rule for  $n = -2$  was introduced by Das, Mathur, and Okubo [4],

$$\text{(WSR 0)} \quad \int_0^\infty ds \frac{\Delta\rho(s)}{s^2} = \frac{1}{3} f_\pi^2 \langle r_\pi^2 \rangle - F_A, \quad (12)$$

where  $\langle r_\pi^2 \rangle$  is the mean squared radius of the charged pion, and  $F_A$  is the coupling constant for the radiative pion decay,  $\pi^\pm \rightarrow \mu^\pm \nu_\mu \gamma$ . We label this sum rule as the 0<sup>th</sup> one since it has a smaller value of  $n$  as compared to Weinberg's initial sum rules. Lastly, Kapusta and Shuryak [5] derived a sum rule for  $n = 1$ ,

$$\text{(WSR 3)} \quad \int_0^\infty ds s \Delta\rho(s) = -2\pi\alpha_s \langle \mathcal{O}_4 \rangle, \quad (13)$$

where  $\langle \mathcal{O}_4 \rangle$  is the part of the four-quark condensate which breaks chiral symmetry. The explicit quark content of this operator is given by

$$\langle \mathcal{O}_4 \rangle = \frac{1}{4} \left( \left\langle (\bar{u}\gamma_\mu\gamma_5\lambda^a u - \bar{d}\gamma_\mu\gamma_5\lambda^a d)^2 - (\bar{u}\gamma_\mu\lambda^a u - \bar{d}\gamma_\mu\lambda^a d)^2 \right\rangle \right), \quad (14)$$

where  $\lambda^a$  denote the Gell-Mann matrices. It is common to assume that this operator can be factorized into the chiral condensate,

$$\langle \mathcal{O}_4 \rangle = \frac{16}{9} \kappa \langle \bar{q}q \rangle^2, \quad (15)$$

where  $\kappa$  is a parameter larger than one to mimic the contributions beyond ground-state saturation. Typically the Weinberg-type sum rules are expressed in vacuum in terms of  $\rho_A$  as is done here. However, it is possible to include the pion pole into the axial-vector spectral function and thereby write the sum rules in terms of  $\bar{\rho}_A$  with their right-hand-side (RHS) appropriately adjusted. This was done in Ref. [5] for the sum rules at finite temperature.

For studies of chiral symmetry restoration, satisfying these sum rules is critical both in medium and in vacuum. In the present work, we will make the first step by using the first three, Eqs. (9), (10), and (12), to constrain the parameters of the vacuum spectral functions. The last sum rule, Eq. (13), is not used due to a large uncertainty in the value of  $\kappa$  and the rather high sensitivity of the integration to large  $s$  where the control from experimental data is limited. Nevertheless, we will still examine how well it is satisfied by the constructed spectral functions.

The QCD sum rules, on the other hand, apply to the vector and axial-vector channels separately. They were first introduced by Shifman, Vainshtein and Zakharov using the operator product expansion (OPE) [7, 8]. They relate the integral over the spectral function to a series of ground-state operators (expectation values) specific for the channel

---

<sup>1</sup> Note that the sum rule in Ref. [30] labeled as Weinberg's 2<sup>nd</sup> sum rule is not the same as the one considered here; the one considered here corresponds to the convergent sum rule in the equal quark-mass limit of Ref. [30].

of interest. To improve the convergence of the integral over the spectral function, one performs a Borel transform on both sides of the sum rule. For the vector channel one obtains

$$\frac{1}{M^2} \int_0^\infty ds \frac{\rho_V(s)}{s} e^{-s/M^2} = \frac{1}{8\pi^2} \left(1 + \frac{\alpha_s}{\pi}\right) + \frac{m_q \langle \bar{q}q \rangle}{M^4} + \frac{1}{24M^4} \langle \frac{\alpha_s}{\pi} G_{\mu\nu}^2 \rangle - \frac{56\pi\alpha_s}{81M^6} \langle \mathcal{O}_4^V \rangle \dots, \quad (16)$$

and for the axial-vector channel

$$\frac{1}{M^2} \int_0^\infty ds \frac{\bar{\rho}_A(s)}{s} e^{-s/M^2} = \frac{1}{8\pi^2} \left(1 + \frac{\alpha_s}{\pi}\right) + \frac{m_q \langle \bar{q}q \rangle}{M^4} + \frac{1}{24M^4} \langle \frac{\alpha_s}{\pi} G_{\mu\nu}^2 \rangle + \frac{88\pi\alpha_s}{81M^6} \langle \mathcal{O}_4^A \rangle \dots \quad (17)$$

By performing the Borel transform, one trades the space-like 4-momentum,  $q^2 = -Q^2$ , with the Borel mass,  $M^2$ . Note that the axial-vector spectral function is defined to contain the contribution from the pion pole (use of  $\bar{\rho}_A$ , not  $\rho_A$ ). To the order  $1/M^6$ , which we are working, the following operators figure: the chiral condensate,  $\langle \bar{q}q \rangle$ , the gluon condensate,  $\langle \frac{\alpha_s}{\pi} G_{\mu\nu}^2 \rangle$ , and the vector and axial-vector four-quark condensates,  $\langle \mathcal{O}_4^V \rangle$  and  $\langle \mathcal{O}_4^A \rangle$ , respectively. The four-quark condensates can be expressed in terms of their quark content as in [19]

$$\langle \mathcal{O}_4^V \rangle = \frac{81}{224} \left\langle (\bar{u}\gamma_\mu\gamma_5\lambda^a u - \bar{d}\gamma_\mu\gamma_5\lambda^a d)^2 \right\rangle + \frac{9}{112} \left\langle (\bar{u}\gamma_\mu\lambda^a u + \bar{d}\gamma_\mu\lambda^a d) \sum_{q=u,d,s} \bar{q}\gamma^\mu\lambda^a q \right\rangle, \quad (18)$$

$$\langle \mathcal{O}_4^A \rangle = -\frac{81}{352} \left\langle (\bar{u}\gamma_\mu\lambda^a u - \bar{d}\gamma_\mu\lambda^a d)^2 \right\rangle - \frac{9}{176} \left\langle (\bar{u}\gamma_\mu\lambda^a u + \bar{d}\gamma_\mu\lambda^a d) \sum_{q=u,d,s} \bar{q}\gamma^\mu\lambda^a q \right\rangle, \quad (19)$$

and are related to the chirally breaking four-quark condensate of Eq. (14) as

$$\langle \mathcal{O}_4 \rangle = \frac{16}{9} \left( \frac{7}{18} \langle \mathcal{O}_4^V \rangle + \frac{11}{18} \langle \mathcal{O}_4^A \rangle \right). \quad (20)$$

These forms of the four-quark condensates and the coefficients in the sum rules are chosen such that  $\langle \mathcal{O}_4^V \rangle$  and  $\langle \mathcal{O}_4^A \rangle$  have a simple factorized form, *viz.*  $\langle \mathcal{O}_4^V \rangle = \kappa_V \langle \bar{q}q \rangle^2$  and  $\langle \mathcal{O}_4^A \rangle = \kappa_A \langle \bar{q}q \rangle^2$ . The parameters  $\kappa_V$  and  $\kappa_A$  are, in principle, independent and thus could take on different values; they are related to  $\kappa$  in Eq. (15) via

$$\kappa = \frac{7}{18} \kappa_V + \frac{11}{18} \kappa_A. \quad (21)$$

For simplicity we have chosen  $\kappa_V$  and  $\kappa_A$  as numerically identical, which then implies from Eq. (21) that  $\kappa$  is also numerically the same, *viz.*  $\kappa_V = \kappa_A = \kappa$ . A more general discussion on the properties of four-quark condensates can be found in [31]. We note that the sign of the chiral-condensate term is the same for the two sum rules, not opposite as one might expect since the chiral condensate is a chirally odd operator. The latter reasoning actually applies to the transverse part of the axial-vector current. However, the QCD sum rule written above is for the total current including the longitudinal part induced by the pion contribution. This leads to the signs presented in Eq. (17). We also note that the Weinberg sum rules 1-3 can be derived from the QCD sum rules by subtracting both sides of the vector and axial-vector QCD sum rules from each other, Taylor expanding the Borel convergence factor  $e^{-s/M^2}$ , and equating the coefficients of equal powers of  $M^2$  on each side. A similar procedure was pointed out in Ref. [8] and used in Ref. [5] to derive Eq. (13).

If one knows the vector or axial-vector spectral function, the QCD sum rule can be used to determine the values of the condensates. Conversely, since the condensates are universal low-energy operators, they can be calculated from other processes, and in turn be used to constrain the spectral functions. Though related to the Weinberg-type, QCD sum rules can provide different constraints on the spectral functions because both chirally even and chirally odd operators are involved. A recent study of the constraints on the spectral functions imposed by the chiral odd operators in the QCD sum rules can be found in Ref. [32]. A potential drawback of the QCD sum rules comes from the relatively large uncertainty of the values of the gluon and 4-quark condensates, as compared with the pion mass or its decay constant in the first three Weinberg sum rules. Therefore, we will not use the QCD sum rules to constrain the vacuum spectral functions, but rather use the constructed spectral functions to constrain the condensates and in this way perform a consistency check.

In principle, there are corrections to the QCD sum rules [7, 8, 33]. Besides the conventional perturbative and power corrections, the most prominent one not included here is associated with the exchange of instantons with the vacuum. It turns out that the importance of instantons depends on the specific correlator [33], *i.e.*, whether direct-instanton interactions are operative, like in the scalar and pseudoscalar meson channels. In both the vector and axial-vector channels these are absent and the remaining corrections are probably small [33]. We therefore believe that the QCD sum rules considered here are sufficiently accurate.

### III. HADRONIC MODELS FOR VECTOR AND AXIAL-VECTOR SPECTRAL FUNCTIONS

So far, we have discussed Weinberg-type and QCD sum rules and their usefulness in constructing vacuum spectral functions. In this section, we present a model which we will use to construct the spectral functions suitable for a physically motivated fit to  $\tau$ -decay data. Note that for the purpose of the present work the concrete fit functions and parameter values are not important as long as the data are accurately reproduced.

Our main ansatz, which is one of the differences of our work from previous analyses, is that the vector and axial-vector spectral functions are divided up into three parts: the ground-state resonance, a first excited state, and a universal continuum,

$$\rho_V(s) = \rho_V^{\text{gs}}(s) + \rho_V^{\text{ex}}(s) + \rho^{\text{cont}}(s) \quad (22)$$

$$\rho_A(s) = \rho_A^{\text{gs}}(s) + \rho_A^{\text{ex}}(s) + \rho^{\text{cont}}(s). \quad (23)$$

The explicit form of each part will be discussed in turn.

The ground-state resonance in the vector channel, the  $\rho(770)$ , has been well-studied in effective hadronic Lagrangians; we here employ the spectral function of Ref. [34] which was originally fit to the pion electromagnetic form-factor and  $P$ -wave  $\pi\pi$  scattering phase shifts, but also turns out to describe the experimental  $\tau$ -decay data well [35]; its medium modifications have been widely applied to experiment, *e.g.*, in dilepton and photon production in heavy-ion collisions [36] and in elementary reactions [37]. These features make the  $\rho$  spectral function a suitable starting point (both in vacuum and for future studies in medium) for the other two components which will largely rely on fits to the  $\tau$ -decay data.

The spectral properties of the  $a_1$  meson are much less studied, especially in the medium. Since our eventual objective are studies of the spectral function's medium modifications (and the pattern of chiral symmetry restoration for the vector and axial-vector), we adopt a more schematic ansatz for the  $a_1$  spectral function. Rather than using the vacuum spectral function from an effective hadronic model (see, *e.g.*, Refs. [38–44]), we employ a generic Breit-Wigner form,

$$\rho_{a_1}(s) = \frac{1}{\pi} \frac{M_{a_1}^4}{g_{a_1}^2} \frac{\sqrt{s} \Gamma_{a_1}(s)}{(s - M_{a_1}^2)^2 + s \Gamma_{a_1}(s)^2}, \quad (24)$$

where  $M_{a_1}$  is the bare mass,  $g_{a_1}$  the axial-vector coupling constant, and  $\Gamma_{a_1}(s)$  the energy dependent width of the resonance. These parameters will be determined uniquely for the  $a_1$ . The form of the coefficient  $M_{a_1}^4/g_{a_1}^2$  is the same as in vector-meson dominance. The energy dependence of the  $a_1$  width will be approximated by an  $S$ -wave decay into  $\rho\pi$ . In order to properly incorporate the three-pion final state, the spectral shape of the  $\rho$  will be accounted for by integrating over its spectral function. Finally, to simulate the finite size of the  $\rho\pi a_1$  vertex and to control the large energy behavior of the  $a_1$  spectral function, a hadronic form-factor is included. Putting all of this together, the energy dependent width of the  $a_1$  takes the form

$$\Gamma_{a_1}(s) = - \int_0^\infty ds' \frac{\text{Im} D_\rho(s')}{\pi} \Gamma_{a_1}^0 \frac{p_{\text{cm}}^{\rho\pi}(s, s')}{p_{\text{cm}}^{\rho\pi}(M_{a_1}^2, s')} \left( \frac{\Lambda_{a_1}^2 + M_{a_1}^2}{\Lambda_{a_1}^2 + s} \right)^2, \quad (25)$$

where  $D_\rho(s)$  is the  $\rho$  propagator, and the center of mass momentum of the  $\rho$  and  $\pi$  decay products,  $p_{\text{cm}}^{\rho\pi}(s, s')$ , is given by

$$p_{\text{cm}}^{\rho\pi}(s, s') = \frac{1}{2} \left( \frac{(s + s' - M_\pi^2)^2 - 4ss'}{s} \right)^{1/2}. \quad (26)$$

This ansatz involves two additional parameters, a form-factor cut-off,  $\Lambda_{a_1}$ , and the  $\rho\pi a_1$  coupling constant which determines the magnitude of the on-shell width,  $\Gamma_{a_1}^0$ , defined as  $\Gamma_{a_1}^0 = \Gamma_{a_1}(M_{a_1}^2)$ .

The first excited resonances in both vector and axial-vector channels, namely the  $\rho'$  and  $a_1'$ , are included in the current construction. Their contribution to the spectral functions is presented here while the motivation will be provided later. Again, we note that not only is this the first attempt to include them in such a study, but given the well established  $\rho'$  contribution, we will be deducing the *need* to include the  $a_1'$  based upon the Weinberg-type sum rules. A microscopic description of the excited resonance states is not well understood to date. Therefore, as was done for the  $a_1$ , the spectral functions of the excited resonances will be approximated by a Breit-Wigner shape as in Eq. (24). To construct the energy-dependent width, we are once again guided by plausible decay channels. However, unlike for the  $a_1$  case, the decay products are not well established. Instead we postulate that the width exhibits a threshold which is controlled by an estimated mass scale. We further postulate that the partial-wave distribution

of the decay products is the same as for its corresponding ground state, namely the  $\rho'$  decays through a  $P$ -wave process while the  $a'_1$  decays through an  $S$ -wave process. Furthermore, since the actual decay products of the excited resonances are not explicitly specified, treating them off-shell by folding in their spectral function is not warranted. As for the ground states, a form-factor will be included. This leads to a width of the  $\rho'$  as

$$\Gamma_{\rho'}(s) = \Gamma_{\rho'}^0 \left( \frac{s - \left(M_{th}^{(\rho')}\right)^2}{M_{\rho'}^2 - \left(M_{th}^{(\rho')}\right)^2} \right)^{3/2} \frac{M_{\rho'}^2}{s} \left( \frac{\Lambda_{\rho'}^2 + M_{\rho'}^2}{\Lambda_{\rho'}^2 + s} \right)^2, \quad (27)$$

and for the  $a'_1$  as

$$\Gamma_{a'_1}(s) = \Gamma_{a'_1}^0 \left( \frac{s - \left(M_{th}^{(a'_1)}\right)^2}{M_{a'_1}^2 - \left(M_{th}^{(a'_1)}\right)^2} \right)^{1/2} \left( \frac{\Lambda_{a'_1}^2 + M_{a'_1}^2}{\Lambda_{a'_1}^2 + s} \right)^2. \quad (28)$$

The parameters  $M_{\rho'}$  and  $M_{a'_1}$  set the bare mass for the pertinent resonances;  $M_{th}^{(\rho')}$  and  $M_{th}^{(a'_1)}$  correspond to the effective mass thresholds of the decay products, while  $\Lambda_{\rho'}$  and  $\Lambda_{a'_1}$  set the form-factor scales. Lastly, the overall strengths of the widths are given by  $\Gamma_{\rho'}^0$  and  $\Gamma_{a'_1}^0$ , which again have been normalized such that  $\Gamma_{\rho'}(M_{\rho'}^2) = \Gamma_{\rho'}^0$  and  $\Gamma_{a'_1}(M_{a'_1}^2) = \Gamma_{a'_1}^0$ .

At high energies, the contribution from the continuum can be calculated from perturbative QCD. Most previous work has assumed that this contribution exhibits a threshold energy below which it vanished while the perturbative value was assumed above. We have adopted a continuous function for all energies which approaches the perturbative value for large energies [5],

$$\rho^{\text{cont}}(s) = \frac{s}{8\pi^2} \left( 1 + \frac{\alpha_s}{\pi} \right) \left( \frac{1}{1 + \exp[(E_{th} - \sqrt{s})/\delta]} \right). \quad (29)$$

The parameter  $E_{th}$  plays the role of a threshold energy while  $\delta$  determines how fast the limiting value is achieved. Furthermore, because at high energies, *i.e.*, in the perturbative regime, QCD is chirally invariant, we postulate an identical continuum contribution to both channels. Thus the parameters  $E_{th}$  and  $\delta$  are the same for the vector and axial-vector channels and  $\rho_V^{\text{cont}} = \rho_A^{\text{cont}}$ . This is the first time that this feature has been implemented; besides the underlying physical motivation of degenerate perturbative continua, it will play a crucial role in interpreting the vacuum spectral functions.

#### IV. VACUUM SPECTRAL FUNCTIONS AND DISCUSSION

The total number of fit parameters of our model for the vector and axial-vector spectral functions in vacuum is 16 (the three from the  $\rho$  spectral function have been fixed before). They include the masses  $M_X$ , the couplings  $g_X$ , the width strengths  $\Gamma_X^0$ , and the form-factors scales  $\Lambda_X$  for each  $X = a_1, \rho'$  and  $a'_1$  states. The  $\rho'$  and  $a'_1$  furthermore incorporate a threshold mass scale,  $M_{th}^{(X)}$ , and finally the continuum carries the two parameters  $E_{th}$  and  $\delta$ . The continuum also depends on the strong coupling constant which was chosen to be  $\alpha_s(1\text{GeV}) = 0.5$ . This set of convenient and physically motivated parameters was determined by fitting the spectral distributions of hadronic  $\tau$ -decays into an even and odd number of pions [11, 12]. In addition, the requirement of reproducing the Weinberg-type sum rules was imposed (except the third one, Eq. (13), *cf.* our comment above). The fit was not done for all 16 parameters simultaneously, but rather three sequential fits were performed. First, the parameters of the  $a_1$  peak and the continuum were determined from the axial-vector ALEPH  $\tau$ -decay data. Second, the  $\rho'$  peak parameters were determined from the vector ALEPH  $\tau$ -decay data. And lastly, the parameters associated with the  $a'_1$  peak were determined from the Weinberg-type sum rules. The parameter values are summarized in Tab. I. Figure 1 shows the resulting spectral functions, divided by  $s$  to render them dimensionless, compared with the experimental data. A measure of the goodness of fit is the coefficient of determination,  $R^2$ . The vector channel has an  $R^2$  value of 0.991 while the axial-vector channel (without the  $a'_1$ ) has an  $R^2$  value of 0.997. Both of these indicate very good agreement of the resulting spectral functions and the experimental data.

The results for the Weinberg-type sum rules are graphically assessed in Fig. 2. Here the left-hand-side (LHS) of each sum rule is plotted as a function of the upper limit of the energy integration. Toward high energies, *i.e.*, when the spectral functions degenerate so that their difference no longer contributes to the sum rule, the curve should

	$a_1$	$\rho'$	$a'_1$
$M_X$	1.246 GeV	1.565 GeV	1.802 GeV
$\Gamma_X^0$	0.612 GeV	0.32 GeV	0.2 GeV
$g_X$	6.15	11.44	28.70
$\Lambda_X$	0.61 GeV	1.41 GeV	1.24 GeV
$M_{th}^{(X)}$	N/A ( $3\pi$ )	0.56 GeV	0.96 GeV

Continuum parameters	
$E_{th}$	1.60 GeV
$\delta$	0.227 GeV

Constant parameters	
$m_\pi$	139.6 MeV
$f_\pi$	92.4 MeV
$m_q$	5 MeV
$\alpha_s(1\text{GeV})$	0.5
$\langle r_\pi^2 \rangle$	0.439 fm <sup>2</sup>
$F_A$	0.0058
$\langle \bar{q}q \rangle$	$(-0.25\text{GeV})^3$

TABLE I: List of parameters of the constructed model as constrained by experimental data and the Weinberg-type sum rules.

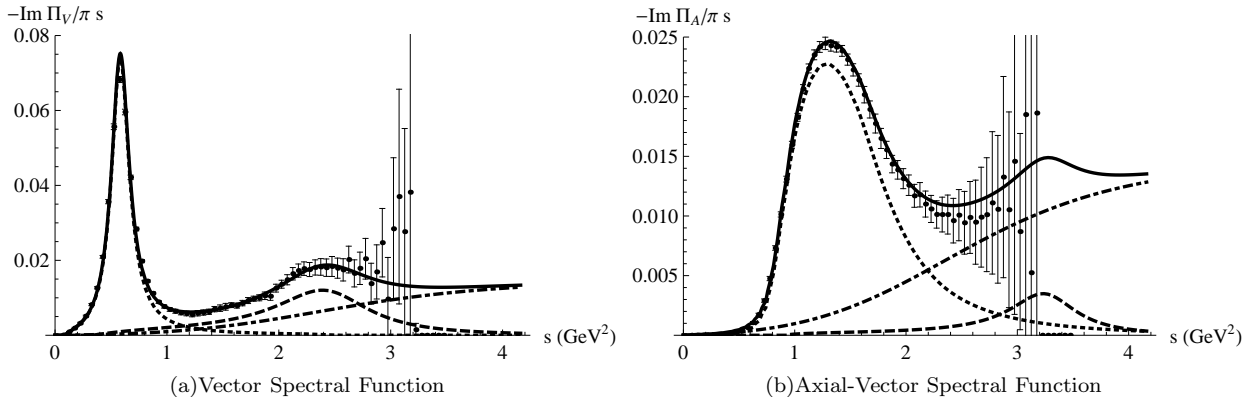


FIG. 1: Spectral functions for the vector (left) and axial-vector channel (right) compared to experimental data for hadronic  $\tau$  decays by the ALEPH collaboration [11]. The different curves highlight the contributions to the total spectral function (solid curve) from the ground-state resonance (dotted curve), the excited resonance (dashed curve), and the continuum (dot-dashed curve).

converge to the value of the RHS, represented by the dashed curve. Table II quantifies the numerical deviation of the asymptotic value from the RHS. The values are quoted such that a positive (negative) deviation means that the contribution from the vector (axial-vector) channel is too large. Primarily by introducing, and then adjusting the mass and the coupling of the  $a'_1$  state, “perfect” numerical agreement with the RHS of Weinberg-type sum rules 1 and 2 can be achieved. This was intentionally done since the respective RHS of these two sum rules are known with much better precision than for WSR-0 and especially WSR-3. Not surprisingly then, the latter exhibits the largest deviation. The value of  $\kappa$  which we use to quantify this deviation is actually determined from the QCD sum rules which will be described in the next section. In all cases, even for WSR-3, the deviation of the converged value from the asymptotic value dictated by the RHS is small compared to the size of the oscillations seen at low energies. The WSR-3 is more sensitive to the higher energy regime as compared to the other sum rules because of the larger power of  $s$  in the integral in Eq. (13). Its deviation suggests that a little less spectral strength is needed in the axial-vector channel at high energies. Nonetheless, the “excess” axial-vector strength in WSR-3 is less than 10% of the total strength generated by the  $a'_1$ . Another possibility is the introduction of a second excited vector state at higher energies; we refrain from this possibility due to the lack of constraints available by the current scheme.

A few comments pertaining to our fit are in order. First, because we have postulated the continuum for the vector and axial-vector spectral functions to be identical, the energy of the effective threshold is larger than in previous applications. This is essentially dictated by the dip region in the axial-vector spectral function data around  $s = 2.2 \text{ GeV}^2$ , which lies below the pQCD continuum level of  $\frac{1}{8\pi^2} (1 + \alpha_s/\pi) \simeq 0.015$ . The onset of the continuum must therefore be pushed out to higher energies to accommodate this dip. This can be observed in Fig. 1(b) by inspecting the contribution from the continuum, the dot-dashed curve. The need for larger  $E_{th}$  may be somewhat mitigated by a tuning of  $\delta$ . By allowing the onset to occur more slowly, *i.e.*, with a larger value of  $\delta$ , a slightly lower onset energy can be obtained. Nevertheless, even with this tuning, the resulting onset energy,  $E_{th}$ , remains significantly larger than in previous studies. Our value for the onset energy might rather be considered as a lower bound, since, in principle, the continuum could be pushed out to even higher energies and compensated by adding further spectral strength to the excited states (*i.e.*, decrease  $g_X$  or adding more states). However, a continuum threshold at even higher energies is

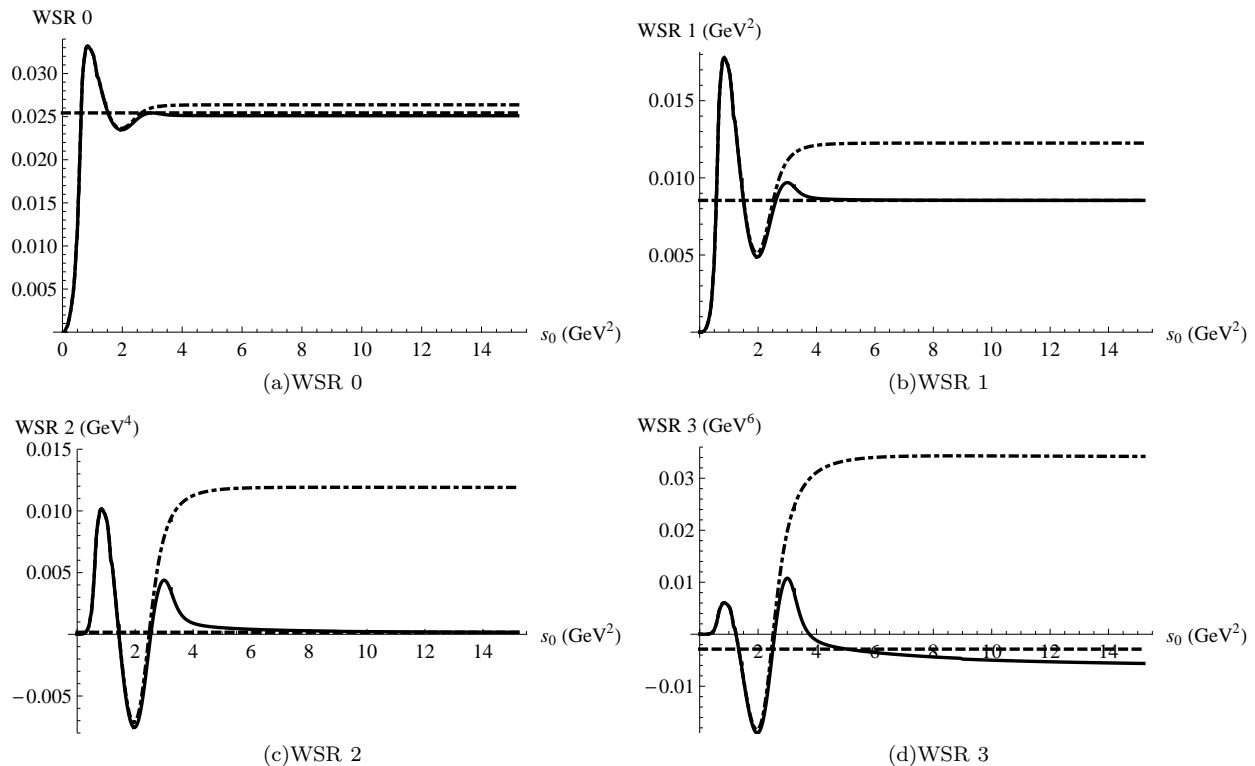


FIG. 2: Graphical representation of the Weinberg-type sum rules. The LHS of Eqs. (9), (10), (12) and (13) is plotted as a function of the upper integration limit (solid curve), compared to the theoretical experimental value for the RHS (dashed curve). The dot-dashed curve is the same as the solid curve but excluding the contribution from the  $a'_1$  state.

WSR	0 <sup>th</sup>	1 <sup>st</sup>	2 <sup>nd</sup>	3 <sup>rd</sup>
% agreement	-1.28%	~ 0%	~ 0%	-96%

TABLE II: Percent disagreement between LHS and the RHS of the Weinberg-type sum rules resulting from our fit.

not well constrained by data. Therefore we have taken the more conservative approach here.

Second, the current study is the first to include excited resonance states into a construction of the spectral functions using sum rule techniques. Previous works [19–21] have argued that their continuum ansatz, with a smaller threshold, was providing sufficient agreement with the data such that explicitly treating these states was not necessary. However, when the continuum is pushed to higher energies, a region in energy is created where the vector spectral function is no longer in good agreement with experiment (*cf.* Fig. 1(a) for the continuum contribution undershooting the data). To accommodate this, it is therefore natural to include the effects of a  $\rho'$  resonance. This argument, based upon *observed* bumps in experimental data, cannot be applied to the axial-vector channel, since there is no direct indication which suggests a clear need for an  $a'_1$  state *a priori*. However, our enforcing of the Weinberg-type sum rules dictates additional strength in the axial-vector channel which is not incompatible with data. To further illustrate this point, let us switch off the  $a'_1$  peak. The resulting axial-vector spectral function still describes the data as seen in Fig. 3, but evaluating the Weinberg-type sum rules in this scenario leads to appreciable discrepancies in all cases, *cf.* the dot-dashed curves in Fig. 2. Therefore, the requirement of satisfying the sum rules by the constructed spectral functions lets us deduce the presence of an  $a'_1$  state.

Third, one may ask if there is other evidence for an excited axial-vector state. The Particle Data Group [24] lists three possible candidates,  $a_1(1640)$ ,  $a_1(1930)$  and  $a_1(2095)$ , though none of them are very well established (the latter two can only be found in the “Further States” list and none are included in the summary table). Being the first excited resonance, it would be natural to associate our  $a'_1$  with the  $a_1(1640)$ , but the mass and width do not match well. A similar problem actually holds for the excited vector resonance: while we fit the ALEPH data with a single  $\rho'$  state of mass 1565 MeV, the PDG has states at  $\rho(1450)$  and  $\rho(1700)$ . This suggests that the bump seen in the data is an amalgamation of the two excited  $\rho$  states. In principle, we could have tried to use a spectral function with two



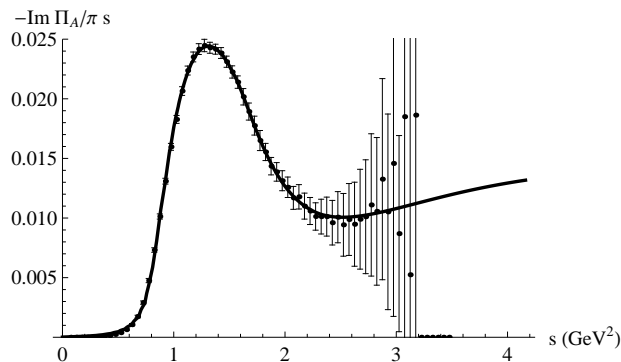


FIG. 3: Spectral function in the axial-vector channel without the  $a'_1$ , compared to experimental data [11].

excited states, but the significance for the latter is not apparent from the single bump in the  $\tau$ -decay data and thus it would only serve to increase the number of our parameters without improving the fit. Though we call our state  $\rho'$ , it may well represent the contribution from the two excited resonance states quoted by the PDG. A similar argument holds for the  $a'_1$  state. It is then not a problem that the properties of this proposed state do not match well with previously seen individual resonances. Nevertheless, it is rather consistent with an average of the lowest two states, similar to the  $\rho'$  case.

Fourth, by adjusting the parameters of the  $a'_1$  states, the percent deviations of the Weinberg-type sum rules can change. The percent deviation of the second Weinberg-type sum rule is the most sensitive to such changes in parameters because the RHS of this sum rule is numerically very small. Each sum rule responds differently to each parameter. For example, the percent deviation of WSR-3 can be decreased by shifting the  $a'_1$  mass to lower energies, however the percent deviation of all the other sum rules becomes worse. As an extreme case, the  $a'_1$  can be shifted to lower energies accompanied by the reduction of the  $a'_1$  coupling so that WSR-2 and WSR-3 are both “precisely” satisfied; WSR-0 and WSR-1 are then violated by  $-2.1\%$  and  $-3.6\%$ , respectively. Although the overall deviations are smaller in this case than with the parameters in Table I, we believe that it is better to get the best possible agreement with the two sum rules which are most accurately known.

Finally, the other fitted parameters seem to be in reasonable agreement with expectations. The  $a_1$  mass is well within the PDG range [24], while its width is at the upper end of its range. The form-factor scales of around 1 GeV are of typical hadronic size, with the one for the  $a_1$  somewhat, though not unreasonably, smaller. The threshold scale is consistent with decays into  $4\pi$  states for the  $\rho'$ , while it is slightly larger than the physically expected  $5\pi$  threshold for the  $a'_1$ . Although the coupling for the  $a'_1$ ,  $g_{a'_1}$ , seems large compared to the other states, its numerical value is dependent on the location of the continuum as discussed above. Overall, the chosen parameters result in spectral functions that fit the data and appear to be within reason of their physical interpretation.

## V. QCD SUM RULES

Although the QCD sum rules were not used to initially constrain the model, it is interesting to determine to what extent the resulting spectral functions satisfy them. From Eqs. (16) and (17), one can see that there are three condensates whose values are needed. The quark condensate will be set at the commonly used value,  $\langle \bar{q}q \rangle = (-0.25 \text{ GeV})^3$ . However, there is appreciable variability in the values of  $\kappa$  and the gluon condensate in the literature. Their values will be tuned to optimize the agreement of the QCD sum rules given our input spectral functions.

To quantify this agreement, we will use the method described in Refs. [17, 18]. In this method, one first defines a LHS and a RHS corresponding to the resonance part in the dispersion integral and the OPE with the continuum contribution from the dispersion integral subtracted, respectively. For our purposes, this division will be written as in Eqs. (16) and (17) with the continuum part of the spectral functions subtracted from both sides. Second, a range in the Borel mass, the so-called Borel window, needs to be established where one expects the best agreement between the two sides given their applicability limitations. We will define the lower limit,  $M_{\min}$ , in the standard way, *i.e.*, as the Borel mass where the terms proportional to  $M^{-6}$  contribute at most 10% to the RHS, indicating that the OPE becomes unreliable at still smaller values of the Borel mass. For large Borel mass, the OPE is dominated by the  $M^0$  term. However, this term is nearly trivially satisfied by the continuum. Therefore, in order to analyze the agreement due to the resonance states, an upper limit to the Borel window is introduced. This is typically chosen as the mass where the continuum contribution equals the one from the resonances. We have found that applying this procedure with our

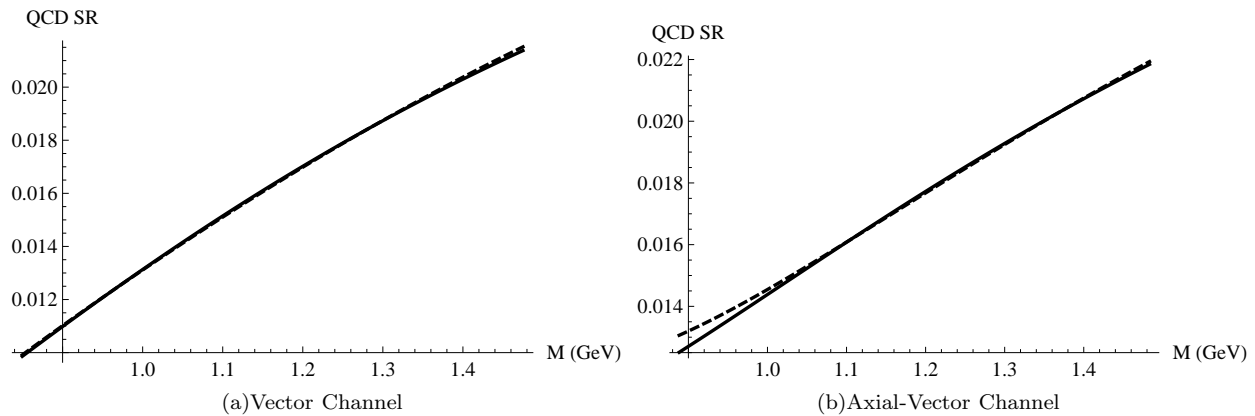


FIG. 4: Graphical representation of the QCD sum rules as a function of Borel mass over the Borel window. The LHS (dispersion integral using the spectral functions of the previous section) of the sum rule is given by the solid curve while the RHS (OPE) is represented by the dashed curve.

spectral functions results in a Borel window nearly double in size of what was previously found in the literature. This difference simply arises due to the significantly higher energies for the onset of our universal continuum. We therefore decided to redefine the upper limit of the window,  $M_{\max}$ , as the mass where the continuum contribution is half of the resonance contribution. This produces a Borel window of similar size as in previous studies. Instead of a 50/50 split between continuum and resonances at the upper range, we thus have a 67/33 proportion between resonances and continuum. With these considerations, we found a Borel window of  $0.85 \text{ GeV} < M < 1.47 \text{ GeV}$  for the vector channel and  $0.89 \text{ GeV} < M < 1.48 \text{ GeV}$  for the axial-vector channel, which is comparable to earlier studies [17–19].

With spectral functions, condensate values, and the Borel window defined, the agreement between the two sides of the sum rule is measured by the value  $d$  defined as

$$d = \frac{1}{\Delta M^2} \int_{M_{\min}^2}^{M_{\max}^2} dM^2 |1 - \text{LHS/RHS}|, \quad (30)$$

where  $\Delta M^2 = M_{\max}^2 - M_{\min}^2$ . One can think of  $d$  as the average deviation between the two sides over the Borel window. The optimization of the values for  $\kappa$  and the gluon condensate thus amounts to minimizing  $d$ . Optimizing the vector and axial-vector channels independently yields different values of  $\kappa$  and the gluon condensate for the two channels. While the gluon condensate should be identical, the value of  $\kappa$ , representing correlations beyond the ground state, can, in principle, be different for different quantum numbers. For simplicity, we have decided to also assume a universal  $\kappa$  value and to minimize the sum of the  $d$  values obtained from the two channels, that is, we minimize  $d_{\text{tot}} = d_V + d_A$ . To estimate the uncertainty in the optimized values, the range in  $\kappa$  and the gluon condensate which produces a combined deviation of less than 1% has been found. The minimization procedure gives  $\kappa = 2.1_{-0.2}^{+0.3}$  and  $\langle \frac{\alpha_s}{\pi} G_{\mu\nu}^2 \rangle = 0.022 \pm 0.002 \text{ GeV}^4$ . The optimized  $d$  values for vector and axial-vector channel are 0.24% and 0.56%, respectively. Increasing the upper limit of the Borel window,  $M_{\max}$  by 5% yields no significant change in the values of the parameters, but increases the deviation. Furthermore, when  $\kappa_V$  and  $\kappa_A$  are decoupled, the optimization procedure yields rather similar results,  $\langle \frac{\alpha_s}{\pi} G_{\mu\nu}^2 \rangle = 0.022 \text{ GeV}^4$ ,  $\kappa_V = 2.1$ ,  $\kappa_A = 2.0$ ,  $d_V = 0.24\%$ , and  $d_A = 0.55\%$ , thereby justifying *a posteriori* the simplifying assumption of identical  $\kappa$  values.

Our values for  $\kappa$  are well within the range previously found in the literature [16, 17, 19, 23], while the value for the gluon condensate is in the upper range. For example, early applications in charmonium sum rules have extracted  $\langle \frac{\alpha_s}{\pi} G_{\mu\nu}^2 \rangle \simeq 0.012 \text{ GeV}^4$  [7]. On the other hand, more recent studies of higher moments of the charmonium sum rules yield significantly larger values, of around  $0.022 \text{ GeV}^4$  [45–47], close to our value.

To illustrate the agreement of the QCD sum rules, we display in Fig. 4 both LHS and RHS for each channel, scaled by  $M^2$ , as a function of  $M$  over the Borel window. With the sub-1% agreement, it is difficult to distinguish the two curves in each figure. We note that an increase in  $\kappa$  with fixed gluon condensate will shift the RHS of the vector channel down, while the RHS of the axial channel is shifted up (dashed curves), thereby making the agreement in both channels worse. Overall, the spectral functions constructed may be considered consistent with the QCD sum rules.

## VI. CONCLUSION

In the present work, we have performed a combined analysis of Weinberg-type and QCD sum rules using vacuum spectral functions for vector and axial-vector channels constructed via quantitative fits to hadronic  $\tau$ -decay data. For the ground-state resonances, we employed a microscopic  $\rho$  spectral function and a Breit-Wigner ansatz for the  $a_1$ . A novel feature of our approach is the introduction of an excited state in each channel which, in turn, allowed us to employ an universal perturbative continuum part at high energies. The universality of the continua is rather welcome in view of chiral degeneracy in perturbation theory, and leads to a higher onset energy than in previous works. While the excited vector state ( $\rho'$ ) was deduced from an accurate fit to data, we have found that the three lowest Weinberg-type sum rules can be quantitatively satisfied only if the existence of an  $a'_1$  state is postulated. The latter lies outside the direct realm of the axial-vector  $\tau$ -decay data, but the extracted mass is compatible with (and in a sense confirms) an average of previously observed states. Furthermore, the resulting spectral functions were implemented into QCD sum rules, resulting in a sub-1% agreement with the operator product expansion (comparable to other state-of-the-art analyses). We believe that these spectral functions provide a good basis for future studies of medium modifications, to shed light on the long-standing problem of testing chiral symmetry restoration with dilepton data.

### Acknowledgments

This work is supported by the US-NSF under grant No. PHY-0969394 and by the A.-v.-Humboldt Foundation (Germany).

- 
- [1] S. Borsanyi *et al.* [Wuppertal-Budapest Collaboration], JHEP **1009** (2010) 073.
  - [2] A. Bazavov, T. Bhattacharya, M. Cheng, C. DeTar, H. T. Ding, S. Gottlieb, R. Gupta and P. Hegde *et al.*, Phys. Rev. D **85** (2012) 054503.
  - [3] S. Weinberg, Phys. Rev. Lett. **18** (1967) 507.
  - [4] T. Das, V. S. Mathur and S. Okubo, Phys. Rev. Lett. **19** (1967) 859.
  - [5] J. I. Kapusta and E. V. Shuryak, Phys. Rev. D **49** (1994) 4694.
  - [6] T. Hilger, B. Kampfer and S. Leupold, Phys. Rev. C **84** (2011) 045202.
  - [7] M. A. Shifman, A. I. Vainshtein and V. I. Zakharov, Nucl. Phys. B **147** (1979) 385.
  - [8] M. A. Shifman, A. I. Vainshtein and V. I. Zakharov, Nucl. Phys. B **147** (1979) 448.
  - [9] R. Rapp, J. Wambach and H. van Hees, in ‘Relativistic Heavy Ion Physics’, Landolt-Boernstein New Series, **I/23A**, 4-1 edited by R. Stock (Springer Verlag, New York, 2010).
  - [10] I. Tserruya, in ‘Relativistic Heavy Ion Physics’, Landolt-Boernstein New Series, **I/23A**, 4-2 edited by R. Stock (Springer Verlag, New York, 2010).
  - [11] R. Barate *et al.* [ALEPH Collaboration], Eur. Phys. J. C **4** (1998) 409.
  - [12] K. Ackerstaff *et al.* [OPAL Collaboration], Eur. Phys. J. C **7** (1999) 571.
  - [13] S. Narison, Nucl. Phys. Proc. Suppl. **96** (2001) 364.
  - [14] C. A. Dominguez and K. Schilcher, Phys. Lett. B **581** (2004) 193.
  - [15] J. Bordes, C. A. Dominguez, J. Penarrocha and K. Schilcher, JHEP **0602** (2006) 037.
  - [16] T. Hatsuda and S. H. Lee, Phys. Rev. C **46** (1992) 34.
  - [17] D. B. Leinweber, Annals Phys. **254** (1997) 328.
  - [18] S. Leupold, W. Peters and U. Mosel, Nucl. Phys. A **628** (1998) 311.
  - [19] S. Leupold, Phys. Rev. C **64** (2001) 015202 [nucl-th/0101013].
  - [20] Y. Kwon, M. Procura and W. Weise, Phys. Rev. C **78** (2008) 055203.
  - [21] Y. Kwon, C. Sasaki and W. Weise, Phys. Rev. C **81** (2010) 065203.
  - [22] M. Asakawa and C.M. Ko, Nucl. Phys. A **560** (1993) 399.
  - [23] F. Klingl, N. Kaiser and W. Weise, Nucl. Phys. A **624** (1997) 527.
  - [24] K. Nakamura *et al.* (Particle Data Group), J. Phys. G **37** (2010) 075021.
  - [25] M. Gell-Mann, R. J. Oakes and B. Renner, Phys. Rev. **175** (1968) 2195.
  - [26] P. Pascual and E. de Rafael, Z. Phys. C **12** (1982) 127.
  - [27] S. Narison, Z. Phys. C **14** (1982) 263.
  - [28] R. D. Peccei and J. Sola, Nucl. Phys. B **281** (1987) 1.
  - [29] V. Dmitrasinovic, Nucl. Phys. A **686** (2001) 379.
  - [30] E. G. Floratos, S. Narison and E. de Rafael, Nucl. Phys. B **155** (1979) 115.
  - [31] R. Thomas, T. Hilger and B. Kampfer, Nucl. Phys. A **795** (2007) 19.
  - [32] T. Hilger, R. Thomas, B. Kampfer and S. Leupold, Phys. Lett. B **709** (2012) 200.
  - [33] V. A. Novikov, M. A. Shifman, A. I. Vainshtein and V. I. Zakharov, Nucl. Phys. B **191** (1981) 301.

- [34] M. Urban, M. Buballa, R. Rapp and J. Wambach, Nucl. Phys. A **673** (2000) 357.
- [35] R. Rapp, Pramana **60** (2003) 675.
- [36] R. Rapp and J. Wambach, Eur. Phys. J. A **6** (1999) 415.
- [37] F. Riek, R. Rapp, T. S. Lee and Y. Oh, Phys. Lett. B **677** (2009) 116.
- [38] Y. Kim, R. Rapp, G. E. Brown and M. Rho, Phys. Rev. C **62** (2000) 015202.
- [39] M. Urban, M. Buballa and J. Wambach, Nucl. Phys. A **697** (2002) 338.
- [40] M. Harada and C. Sasaki, Phys. Rev. D **73** (2006) 036001.
- [41] M. Wagner and S. Leupold, Phys. Lett. B **670** (2008) 22.
- [42] S. Struber and D. H. Rischke, Phys. Rev. D **77** (2008) 085004.
- [43] M. Wagner and S. Leupold, Phys. Rev. D **78** (2008) 053001.
- [44] D. Cabrera, D. Jido, R. Rapp and L. Roca, Prog. Theor. Phys. **123** (2010) 719.
- [45] S. Narison, Phys. Lett. B **387** (1996) 162.
- [46] S. Narison, Phys. Lett. B **706** (2012) 412.
- [47] S. Narison, Phys. Lett. B **707** (2012) 259.